ORIGINAL RESEARCH

Temperature-Dependent Aggregation of Tau Protein Is Attenuated by Native PLGA Nanoparticles Under in vitro Conditions

Pallabi Sil Paul[1], Mallesh Rathnam[1], Aria Khalili[2], Leonardo M Cortez[1], Mahalashmi Srinivasan[3], Emmanuel Planel[4], Jae-Young Cho [2,5], Holger Wille [3], Valerie L Sim[1], Sue-Ann Mok[3], Satyabrata Kar [1]

[1]Department of Medicine (Neurology), Centre for Prions and Protein Folding Diseases, University of Alberta, Edmonton, Alberta, T6G 2M8, Canada; [2]Quantum and Nanotechnology Research Centre, National Research Council Canada, Edmonton, Alberta, Canada; [3]Department of Biochemistry, Centre for Prions and Protein Folding Diseases, University of Alberta, Edmonton, Alberta, Canada; [4]Department of Psychiatry and Neurosciences, University of Laval, Quebec, Canada; [5]Department of Mechanical Engineering, University of Alberta, Edmonton, Alberta, Canada

Correspondence: Satyabrata Kar, Department of Medicine (Neurology), Centre for Prions and Protein Folding Diseases, University of Alberta, Edmonton, Alberta, T6G 2M8, Canada, Tel +1-780-492-9357, Fax +1-780-492-9352, Email skar@ualberta.ca

Introduction: Hyperphosphorylation and aggregation of the microtubule-associated tau protein, which plays a critical role in many neurodegenerative diseases (ie, tauopathies) including Alzheimer's disease (AD), are known to be regulated by a variety of environmental factors including temperature. In this study we evaluated the effects of FDA-approved poly (D,L-lactide-co-glycolic) acid (PLGA) nanoparticles, which can inhibit amyloid-β aggregation/toxicity in cellular/animal models of AD, on temperature-dependent aggregation of 0N4R tau isoforms in vitro.

Methods: We have used a variety of biophysical (Thioflavin T kinetics, dynamic light scattering and asymmetric-flow field-flow fractionation), structural (fluorescence imaging and transmission electron microscopy) and biochemical (Filter-trap assay and detection of soluble protein) approaches, to evaluate the effects of native PLGA nanoparticles on the temperature-dependent tau aggregation.

Results: Our results show that the aggregation propensity of 0N4R tau increases significantly in a dose-dependent manner with a rise in temperature from 27°C to 40°C, as measured by lag time and aggregation rate. Additionally, the aggregation of 2N4R tau increases in a dose-dependent manner. Native PLGA significantly inhibits tau aggregation at all temperatures in a concentration-dependent manner, possibly by interacting with the aggregation-prone hydrophobic hexapeptide motifs of tau. Additionally, native PLGA is able to trigger disassembly of preformed 0N4R tau aggregates as a function of temperature from 27°C to 40°C.

Conclusion: These results, taken together, suggest that native PLGA nanoparticles can not only attenuate temperature-dependent tau aggregation but also promote disassembly of preformed aggregates, which increased with a rise of temperature. Given the evidence that temperature can influence tau pathology, we believe that native PLGA may have a unique potential to regulate tau abnormalities associated with AD-related pathology.

Keywords: tau protein, PLGA nanoparticles, tau pathology, protein aggregation

Introduction

Tau is a soluble microtubule-associated protein that plays an important role in cytoskeletal stability and intracellular trafficking. In the adult human brain, tau comprises six different isoforms ranging from 352 to 441 amino acids, generated by alternative splicing of the microtubule associated protein tau (*MAPT*) gene located on chromosome 17. The isoforms generated by splicing exons 2 and 3 lead to the absence or presence of 1 or 2 N-terminal repeats (0N, 1N or 2N) and splicing of exon 10 results in tau containing 3- or 4-repeats (3R or 4R) of the microtubule binding site.[1,2] Structurally, full-length tau contains four distinct domains: the N-terminal domain (NTD), the proline-rich domain (PRD), the microtubule binding domain (MTBD) and the C-terminal domain (CTD). Compared to 3R tau, 4R tau contains one additional microtubule binding repeat and thus promotes microtubule assembly more efficiently.[1–3] At the

Graphical Abstract
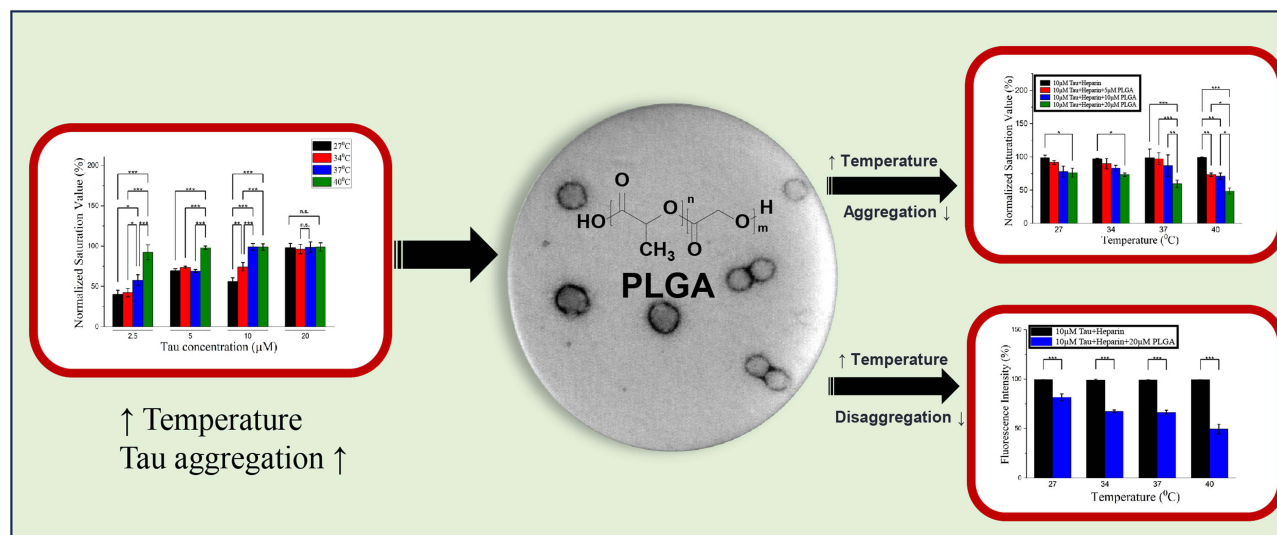
cellular level, tau is found mostly in neurons and to a lesser degree in astrocytes and oligodendrocytes. Physiologically, tau binds and stabilizes microtubules via a site-specific phosphorylation-dephosphorylation process mediated by multiple kinases and phosphatases, respectively.[2,4] However, hyperphosphorylation promotes detachment of tau from microtubules, leading to fibrillization into single straight/paired helical filaments (PHFs) which trigger the formation of intracellular neurofibrillary tangles (NFTs). This, in turn, results in the loss of neurons in a variety of neurodegenerative diseases collectively called "tauopathies", including Alzheimer's disease (AD), frontotemporal lobar degeneration and Pick disease. Most of these diseases, unlike AD, are associated with mutations of the *MAPT* gene and occur without extracellular β-amyloid (Aβ)-containing neuritic plaques.[5–8] Mounting evidence suggests that conversion of tau from a soluble monomer into oligomers/aggregates plays a critical role not only in the loss of neurons but also in the "seed-induced" spreading of disease pathology.[7,9–12] Thus, preventing hyperphosphorylation and/or aggregation of tau is a promising strategy for averting or delaying the onset of tauopathies.

Under normal conditions, wild-type tau usually does not aggregate, but alterations in the MTBD initiated by post-translational modifications such as phosphorylation, acetylation, methylation or glycation can trigger conversion of soluble monomeric tau into pathological aggregates.[13–15] The conformational transition can also be influenced by a variety of environmental factors including pH, metal ions, ionic strength and temperature.[16–19] There is evidence that temperature can influence tau phosphorylation/aggregation in a variety of conditions; decreasing temperature by $<1°C$ below the physiological range has been shown to increase tau phosphorylation in cultured cells/neurons.[20–22] Variation in body temperatures has also been shown to influence tau phosphorylation in wild-type animals[20,23] and affect tau pathology in animal models of tauopathies including AD.[24–26] The body temperature in healthy humans varies between 35 and 39°C and can increase up to 42°C during fever,[27,28] but local temperature in different brain diseases/tumors ranges between 33.4 and 42°C.[29–31] There is evidence from clinical studies that high temperature-associated sauna baths may lower the risk of developing AD pathology,[32] while lower body temperature is linked to increased tau pathology.[33] A number of studies indicate that anesthesia/hibernation that reduces core body temperature, can increase tau phosphorylation,[33–38] whereas increasing body temperature differentially affects tau phosphorylation/pathology in cellular and animal models.[22,39] Although these studies suggest an alteration in temperature homeostasis can regulate tau phosphorylation/aggregation, very little is known how small molecular agents/drugs, as a function of temperature, can influence tau aggregation kinetics that might mitigate/delay disease pathology.

Over the last decade, various nanoparticles synthesized from natural or synthetic polymers have generated a lot of interest in the field of nanomedicine due to their unique structural stability, high surface area-to-volume ratio and ease of surface functionalization.[40–44] Among numerous polymeric nanoparticles, poly(lactic-co-glycolic) acid (PLGA), a family of FDA-approved biodegradable polymers synthesized from glycolic acid and lactic acid, has become ubiquitous as a delivery vehicle for numerous drugs, proteins and other macromolecules because of its biocompatibility and excellent safety profile.[45–49] There is evidence that PLGA nanoparticles are able to cross the blood-brain barrier to deliver drugs that modify disease pathology.[50–53] In fact, some studies have reported that PLGA-encapsulated drugs/agents such as curcumin, nicotinamide, methylene blue, quercetin and polyphenols can attenuate tau aggregation/pathology not only in cultured cells but also in animal models of neurodegenerative diseases after crossing the blood-brain barrier.[54–59] Interestingly, we recently reported that PLGA nanoparticles without conjugation to any agent/drug (ie, native PLGA) can attenuate Aβ aggregation/toxicity in cellular and animal models of AD.[60–62] We also showed that native PLGA can suppress Aβ seed-induced tau aggregation in an in vitro paradigm not only by prolonging the lag phase but also attenuating the growth and saturation of tau fibrils. At present, precise mechanisms causing these effects remain unclear, but the inhibitory effect of PLGA on tau aggregation could be either due to i) interaction of PLGA with Aβ seeds precluding the hydrophobic contacts required for template-assisted tau fibril formation or ii) interaction of PLGA with the Aβ core region that can influence the aggregation prone "VQIINK" and "VQIVYK" regions of tau resulting, in the destabilization of aggregation kinetics.[63] In the present study, we evaluated the effects of native PLGA on temperature-dependent aggregation kinetics of tau protein, which may influence the development/treatment of various tauopathies including AD.

Materials and Methods

Materials

PLGA (50:50 resomer, mol. wt. ~30,000) was purchased from Phosphorex (Hopkinton, MA, USA), whereas Thioflavin T (ThT), dithiothreitol (DTT), Dulbecco's phosphate-buffered saline (PBS), heparin sodium salt and 8-anilino-1-naphtha-lene sulfonate (ANS) were from Sigma-Aldrich (St. Louis, MO, USA). The bicinchoninic acid (BCA) protein assay kit and enhanced chemiluminescence (ECL) kit were from Thermo Fisher Scientific Inc. (Nepean, ON, Canada). Electron microscopy grids (carbon-coated 400 mesh copper grids) and uranyl acid stains were from Electron Microscopy Sciences (Hatfield, PA, USA). Human recombinant 2N4R tau was obtained from StressMarq biosciences Inc. (Victoria, BC, Canada). The primary antibodies, ie, anti-tau1-223, anti-tau316-355 and anti-tau368-441 were from the BioLegend (San Diego, CA, USA), whereas anti-tau oligomeric antibody was from EMD Millipore (Oakville, ON, Canada). The horseradish peroxidase-conjugated secondary antibodies were from Bio-Rad Lab (Hercules, CA, USA). All other chemicals were from either Sigma-Aldrich or Thermo Fisher Scientific.

Preparation and Purification of Human Recombinant Tau

Human recombinant 0N4R tau was prepared and purified following our previously reported established methods.[64] In brief, the expression of 0N4R tau in *E. coli* was induced in a medium comprising terrific broth, 10mM betaine and 500mM NaCl. Induction was achieved using 500μM isopropyl-thio-β-d-galactoside for 3hrs at 30°C. Subsequently, cells were lysed via a microfluidizer and the resulting cell lysate was subjected to boiling. The clarified supernatant containing soluble tau was subjected to cation exchange chromatography (20mM MES pH 6.8, 2mM DTT, 1mM MgCl$_2$, 1mM EGTA, 50–600mM NaCl). Purified tau fractions were pooled and dialyzed into an aggregation assay buffer containing PBS (pH 7.4) with 2mM DTT. The protein was then concentrated using a 3kDa MWCO filter and its concentration was determined using a Pierce™ BCA Protein Assay Kit - Reducing Agent Compatible. Purified protein aliquots were stored at −80°C until use.

Preparation of PLGA Nanoparticles

PLGA nanoparticles were prepared following the manufacturer's instructions as described earlier.[61,62] Briefly, PLGA powder was dissolved in 0.01M PBS (pH 7.4) and subjected to sonication utilizing a probe sonicator with 40 pulses at 40% amplitude prior to using in various experiments.

In vitro Tau Aggregation

Aggregation kinetic assays for wild-type 0N4R Tau (2.5–20μM) were conducted in 150μL of assay buffer (Dulbecco's PBS, 2mM $MgCl_2$, 1mM DTT, pH 7.2) at temperatures of 27°C, 34°C, 37°C and 40°C. In parallel, we evaluated the aggregation kinetics of 2N4R tau (5–20μM) at 37°C under the same conditions. Heparin sodium salt (final concentration of 0.044 mg/mL) was included in the assays, both in the absence and presence of varying concentrations (5μM, 10μM or 20μM) of PLGA. In the uninduced controls, assay buffer was used in place of the heparin solution. The aggregation process was continuously monitored using a ThT binding assay, with ThT concentration maintained at 20μM throughout the experiment. Fluorescence signals were recorded at 15min intervals for 40hrs using a Fluostar Omega BMG Labtech instrument (Aylesbury, UK) with excitation at 440nm, emission at 480nm and a 475nm emission cutoff. For disassembly experiments, the ThT signal was recorded for matured 0N4R tau aggregates, with or without the addition of 20μM PLGA, over 60hr period. The lag time of tau aggregation under various conditions was determined by selecting a common fraction of fluorescence signal intensity (ie, 5%) relative to the pre-transition baseline, following a previously established method.[63,65] All kinetic experiments were repeated three times, with six technical replicates for each sample/experiment, and the data are presented as mean ± SEM for each condition. Raw data from the experiments were normalized as a percentage of fluorescence intensity and the graphs were generated using ORIGIN 2018.

Detection of Soluble Tau Using BCA Assay

To validate our tau ThT kinetic assay, we performed the colorimetric BCA assay to detect the presence of total soluble 0N4R tau following interaction with PLGA as described earlier.[66] In brief, 10μM tau was incubated in the presence of heparin (0.044μg/mL) with 5, 10 or 20μM PLGA for 60hr at different temperatures (ie, 27, 34, 37 and 40°C). As control, 10μM tau was incubated with heparin for 60hr at different temperatures. Subsequently, all samples were centrifuged at 14,000rpm for 30min, and 50μL supernatant from each sample were processed in triplicate in 96 well-plates to measure soluble tau protein. For the positive control (100% soluble tau), we prepared 10μM tau immediately without adding heparin, and 50μL samples in triplicate were loaded into 96 well-plates. We then added 200μL BCA reagent to each well and incubated for 30min at 37°C. After the incubation, the absorbance was measured at 562nm using a Spectramax M5 multi-plate reader and the data were plotted by using Origin 2018 software.

Fluorescence Microscopy

A small aliquot (10μL) of the 0N4R and 2N4R tau samples from various experimental conditions, in the presence or absence of PLGA, was applied to a clean glass slide, air-dried and subsequently stained with ThT solution as previously described.[62,67] Images of ThT-stained 0N4R and 2N4R tau aggregates were captured using a Nikon Eclipse 90i fluorescence microscope at 20X magnification.

Scanning Transmission Electron Microscopy (STEM)

An ultra-high resolution Hitachi S-5500 cold field emission STEM was employed to assess the morphological alterations of 0N4R tau samples acquired from diverse experimental approaches. In the initial phase, 5μL aggregated tau samples with or without PLGA, were carefully placed onto plasma-cleaned, carbon-coated copper grids for a duration of 30sec. Excess liquid was gently removed through blotting, and the grids were allowed to air-dry. Following this, a gentle wash with 10μL of Milli-Q water was performed to eliminate any residual salt. Subsequently, the grids were stained for 30sec using a 2% aqueous uranyl acetate solution, followed by blotting to remove excess liquid. After drying, the grids were imaged using a 30kV accelerating voltage and a 30μA emission current as described earlier.[62]

Dynamic Light Scattering (DLS)

Using a Malvern Zetasizer-Nano Instrument the size distribution of aggregated 0N4R and 2N4R tau samples, with or without PLGA, was analyzed after 40 or 60hrs as described recently.[63,67] A He-Ne laser with a wavelength of 632nm was used to detect backscattered light at a fixed angle of 173°. Tau samples were prepared by shaking 10μM tau with heparin and PLGA (5–20μM) at temperatures of 27°C, 34°C, 37°C and 40°C. The software (DTS v6.20) determined mean size and polydispersity. Assuming water-like properties, with a refractive index of 1.33, data were collected from a minimum number of 10 consecutive runs of 10sec each using a 10mm quartz cuvette filled with 150μL sample without agitation to obtain the auto-correlation function. Particle size was deduced via the Stokes-Einstein equation in the provided software.

8-Anilino-1-Naphthalene Sulfonate (ANS) Binding Assay

The ANS binding assay is a standard method used for detecting protein aggregation.[67] In brief, 10μM ANS was added to aggregated 0N4R tau samples with or without 20μM PLGA, incubated for 30min in a light-shielded environment and then emission spectra were recorded between 400 and 700nm using a Spectramax M5 multi-plate reader followed by excitation at 380nm. For data evaluation, ANS emission spectra in buffer were subtracted from the corresponding ANS/ protein spectra. This procedure was repeated three to four times and then the mean results were plotted using ORIGIN 2018 software.

Asymmetric-Flow Field-Flow Fractionation (AF4)

AF4 assay was used as described earlier[68] to validate our monomeric, oligomeric and fibrillar 0N4R tau preparations. In brief, while monomeric tau (10μM) was prepared in the absence of heparin, oligomeric and fibrillar conformations were generated by incubating tau (10μM) in the presence of heparin (0.044mg/mL) for 24hr at 4°C and 72hr at 37°C, respectively. To validate conformations, different tau isoforms were subjected to AF4 on an Eclipse system (Wyatt Technology) using PBS (pH 7.4) as the running buffer. The channel was 27cm in length and 400μm in height and lined with a 10kDa cutoff polyethersulfone membrane at the accumulation wall. Samples were focused for 5min and then eluted at a channel flow of 0.5mL/min with constant cross-flow of 3mL/min for the first 20min, decreasing from 3 to 0.15mL/min in the following 10min, from 0.15 to 0mL/min in the next 12min, and run with no cross-flow for the last 10min. Multi-angle light scattering and DLS were collected simultaneously in the in-line DAWN HELEOS II detector (Wyatt Technology), operating at a wavelength of 662nm. Data analysis was performed with ASTRA 8.1.2 software (Wyatt Technology).

Filter-Trap Assay

To identify the interaction between tau conformers and PLGA, monomeric, oligomeric and fibrillar 0N4R tau were incubated with or without PLGA and processed for a filter-trap assay, employing four different tau antibodies. In brief, 10μM tau in the presence of heparin was incubated with or without 20μM PLGA either for 24hr at 4°C or for 72hr at 37°C to define interaction with oligomeric and fibrillar conformations, respectively. To measure interaction with monomeric tau, 10μM tau in the absence of heparin was incubated with or without 20μM PLGA briefly at room temperature. Treated and untreated tau samples (20μL) were then loaded onto a 0.02μm nitrocellulose membrane and subjected to vacuum filtration by using a 96-well Bio-Dot Microfiltration system.[62] The membranes were then washed with 1X TBST (0.2% Tween 20), blocked with 5% BSA for 2hr at room temperature and incubated overnight at 4°C with sequence specific anti-tau1-223 (1:1000), anti-tau316-355 (1:1000), anti-tau368-411 (1:1000) and oligomer specific anti-tau T22 (1:1000) antibodies. Subsequently, membranes were washed 1X TBST, treated with appropriate HRP-conjugated secondary antibodies (1:1000) for 2hr at room temperature and developed using ECL kit. All the membranes were stained with Ponceau to determine sample loading, examined by using a FluorChem E system (Santa Clara, CA, USA) and the images were processed using Image J software.

Statistical Analysis

All kinetic data collected from a minimum of 3–5 biological repeats, with each experiment performed in six technical replicates, were expressed as means ± SEM. The data were analyzed by one-way ANOVA followed by Tukey's *post-hoc* analysis for paired comparisons with a significance threshold set at $p < 0.05$. P values indicate the following significances: *$p < 0.05$; **$p < 0.01$ and ***$p < 0.001$. All statistical analyses were performed using ORIGIN software.

Results

Effects of Temperature on Tau Aggregation

The aggregation of the tau protein is a fundamental process linked to tau pathology and is a hallmark of several neurodegenerative diseases. Tau fibrils exhibit a repetitive cross-β sheet structure stabilized by various molecular interactions.[4,7,11] The established fluorescent dye ThT is often used to detect tau fibril formation as it emits strong fluorescence upon binding to cross-β fibril structures.[69] Since temperature influences aggregation of various proteins and also tau phosphorylation, which plays a critical role in the development of AD-related pathology,[21,37,70,71] we evaluated first how alteration in temperature can influence tau aggregation under in vitro conditions (Figure 1A–V). Thus, we performed ThT kinetic assays using 2.5–20μM 0N4R human tau in the presence of heparin at four different temperatures (27, 34, 37 and 40°C) over a 40hr period. The observed aggregation kinetics consistently displayed sigmoidal curves, characterized by a lag phase, an exponential phase followed by a saturation phase (Figure 1A, F, K and P). An increase in temperature from 27°C to 40°C led to a significant reduction in the lag time (Figure 1U), an increase in the aggregation rate (reflected in the slope of the exponential phase of the kinetic curve) and formation of tau fibrils at each concentration studied (Figure 1A, F, K, P and V). The kinetic changes were more pronounced at 2.5 and 5μM compared to 10 or 20μM tau over the 40hr incubation period. Additionally, temperature variations significantly altered ThT fluorescence values at saturation more markedly at 2.5 and 5μM than at 20μM concentrations of tau over the 40hr incubation period. However, temperature increase, irrespective of the studied concentration, was found to enhance formation of tau fibrils at the assay end point, as evident from our fluorescence imaging of ThT-labelled tau samples (Figure 1B–E, G–J, L–O and Q–T). The propensity of tau to aggregate was also apparent from our STEM images and DLS analysis (Figure 2A–T). While STEM images depicted a gradual increase in the size of aggregates with increasing temperature (Figure 2A–D, F–I, K–N and P–S), our DLS analysis showed a significant enhancement in the hydrodynamic radius of tau aggregates as a function of temperature, at a given concentration (Figure 2E, J, O and T). In parallel, we showed that aggregation of 5–20μM 2N4R tau also increased in a dose-dependent manner as evident from our ThT kinetic assays, fluorescence imaging and DLS analysis (Supplementary Figure 1A–D).

Effect of PLGA on Temperature-Dependent Spontaneous Tau Aggregation

Before exploring the effect of native PLGA on tau aggregation, we showed that PLGA, as reported earlier,[61,62] exhibits spheroidal morphology with ~100nm diameter in STEM and DLS analyses, respectively (Supplementary Figure 2). We have recently reported that PLGA is stable over a 48hr period at 27°, 37° and 40°C.[62] Consequently, we assessed the effects of 5, 10 and 20μM native PLGA on the aggregation kinetics of 10μM 0N4R tau at 27°, 34°, 37° and 40°C over a 40hr period (Figure 3A–V). Our ThT kinetics results clearly demonstrated that spontaneous tau aggregation across all temperatures was significantly attenuated in a dose-dependent manner by native PLGA (Figure 3A, F, K and P). At lower concentrations of 5 and 10μM, where the PLGA:tau ratios were 0.5:1 and 1:1, respectively, PLGA exhibited a significant *albeit* modest inhibitory effect on tau aggregation at differing temperatures. Conversely, with a higher concentration (ie, 20μM; PLGA:tau ratio of 2:1) a pronounced inhibition of tau aggregation was evident across all temperatures: a reduction of ~24% at 27°C, ~27% at 34°C, ~40% at 37°C and ~51% at 40°C at saturation over the 40hr incubation (Figure 3A, F, K, P and V). Increasing PLGA concentrations were associated with a significant increase in lag times and reduced rates of tau fibrilization at all temperatures, with the most pronounced effects seen at 37°C and 40°C (Figure 3A, F, K, P and U). The inhibitory influence of native PLGA on 0N4R tau aggregation was further validated using fluorescence imaging, which revealed a decrease in the number and length of tau fibrillar entities in the presence of native PLGA (Figure 3B, C, G, H, L, M, Q and R) with a rise of temperature from 27°C to 40°C.
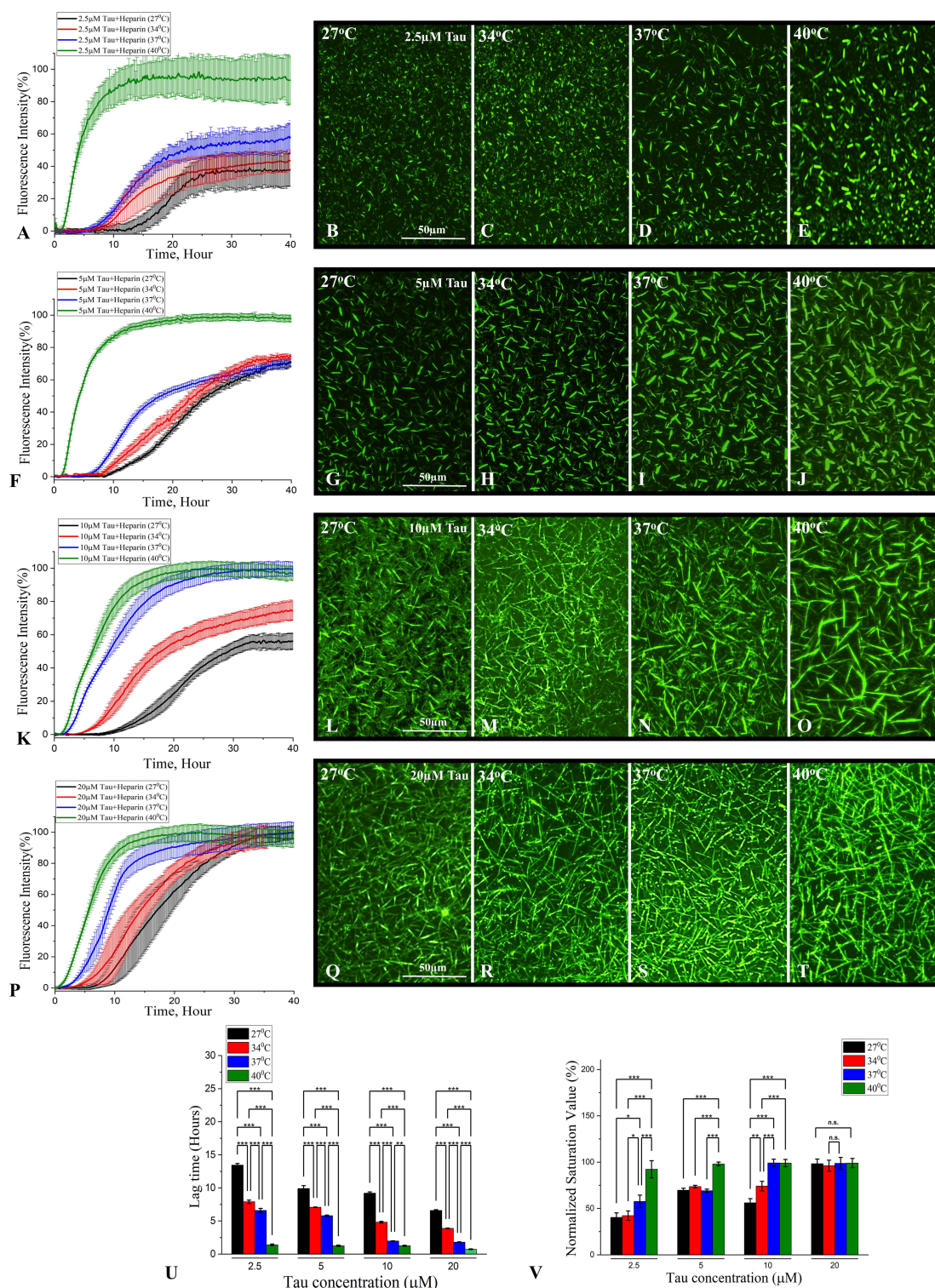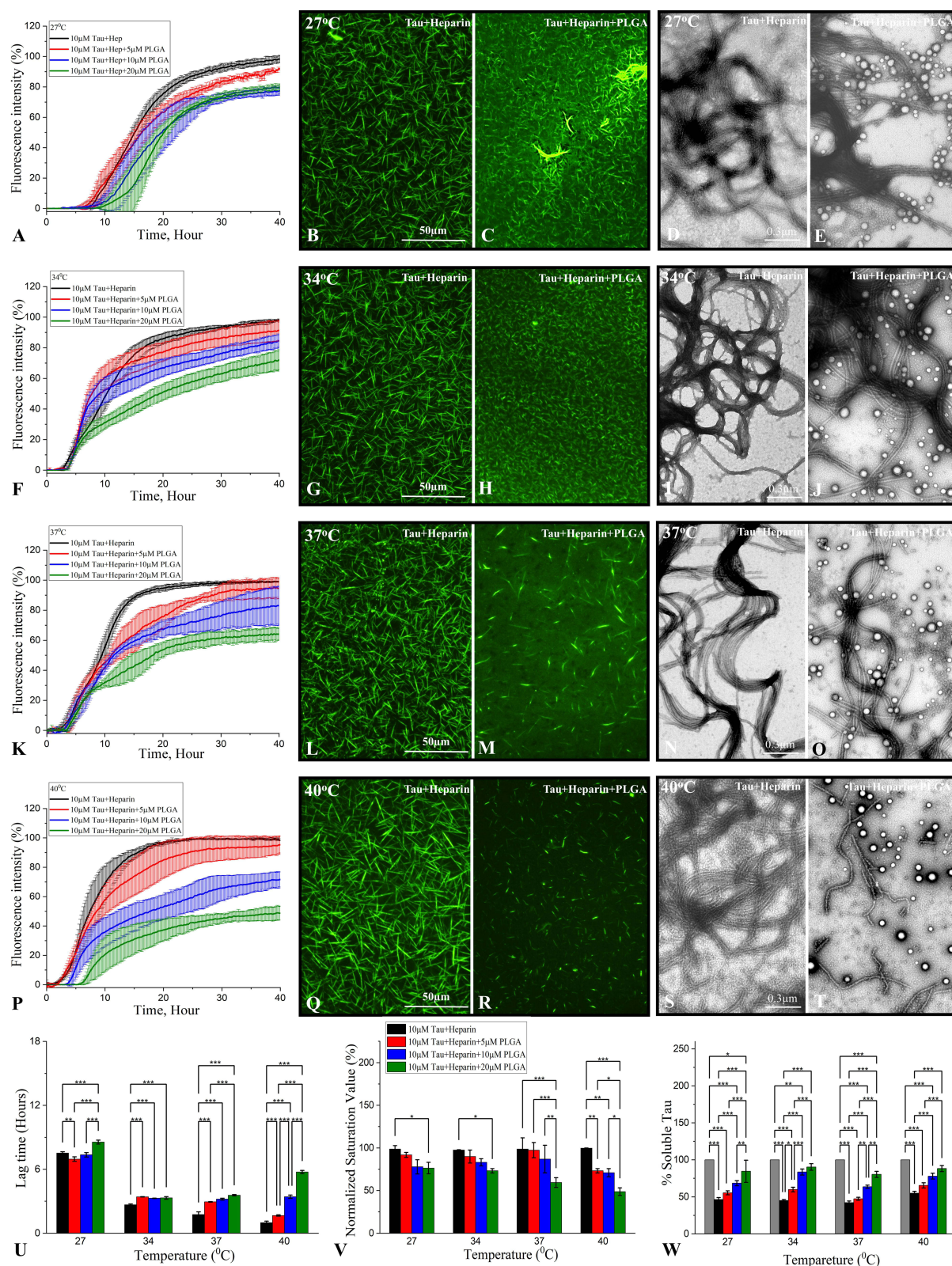
Figure 1 Aggregation of Tau in the presence of heparin at different temperatures. (**A–T**) ThT fluorescence kinetic assays showing the aggregation curves and the corresponding fluorescence images of 2.5μM (**A–E**), 5μM (**F–J**), 10μM (**K–O**) and 20μM (**P–T**) tau in the presence of heparin over a 40hr incubation period at 27°C, 34°C, 37°C and 40°C. Note the aggregation of 0N4R tau increases as functions of dose and temperature and plateaus over time as indicated by ThT fluorescence levels. The fluorescence images of tau fibrils at different concentrations were taken following 40hr incubation at 27°C, 34°C, 37°C and 40°C. (**U** and **V**) Histograms showing the significant reduction of lag-time at various concentrations (2.5–10μM) of tau with the rise of temperature (**U**) and the significant increase in final fluorescence values of various concentrations of tau with the rise of temperatures from 27°C to 40°C (**V**). All ThT kinetic graphs represented average mean ± SEM of three separate experiments, each performed with six replicates for each condition. n.s. represent non significant. *$p < 0.05$, **$p < 0.01$, ***$p < 0.001$.
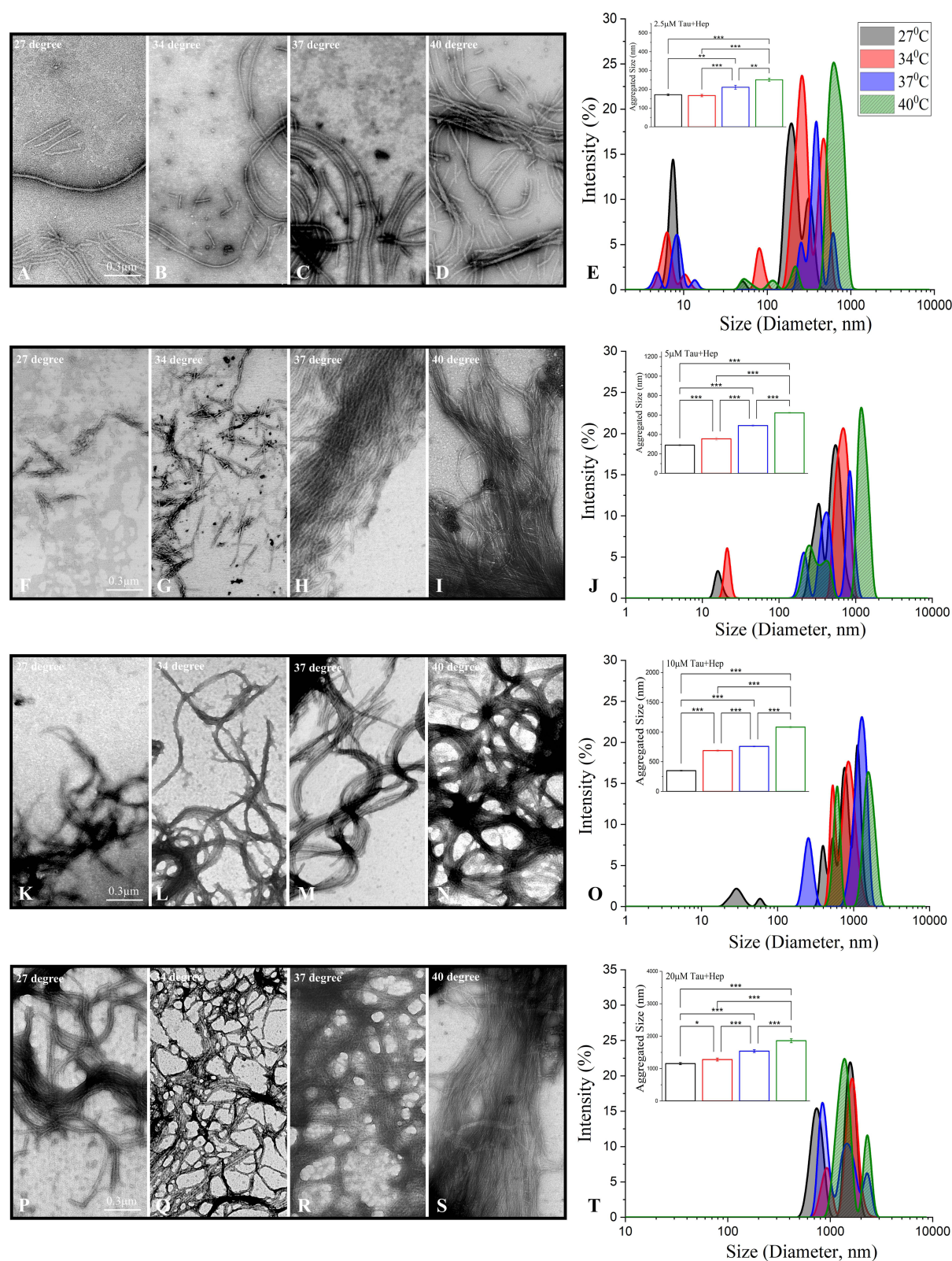
Figure 2 STEM and DLS analysis of tau aggregation at different temperatures. (**A–T**) STEM images and DLS analysis of 2.5µM (**A–E**), 5µM (**F–J**), 10µM (**K–O**) and 20µM (**P–T**) 0N4R tau in the presence of heparin over 40hr incubation at 27°C, 34°C, 37°C and 40°C. Note an increase in the aggregation, as revealed by STEM images, at each concentration of tau with the rise of temperature from 27°C to 40°C. DLS analysis showing variable significant increases in the diameter of aggregated tau at 2.5µM (**E**), 5µM (**J**), 10µM (**O**) and 20µM (**T**) with the rise of temperature from 27°C to 40°C following 40hr incubation as depicted by size distribution curves and histograms (insets) representing average aggregate sizes of tau aggregates for a given concentration. $*p < 0.05$, $**p < 0.01$, $***p < 0.001$.

Figure 3 Attenuation of tau aggregation by PLGA at different temperatures. (**A**–**W**) PLGA dose-dependently (5–20μM) attenuates aggregation propensity of 10μM 0N4R tau as revealed by ThT kinetic assays and respective fluorescence as well as STEM images over 40hr incubation at 27°C (**A**–**E**), 34°C (**F**–**J**), 37°C (**K**–**O**) and 40°C (**P**–**T**). (**U** and **V**) Histograms representing the significantly attenuated fluorescence values at lag-time (**U**) and at saturation (**V**) of tau kinetic reaction in the absence and presence of 5–25μM PLGA at different temperatures. (**W**) Histograms showing the significant increase in the levels of soluble tau, as revealed using the BCA assay, at saturation of the tau kinetic reaction in the absence and presence of 5–20μM PLGA at different temperatures. All ThT kinetic graphs represented average mean ± SEM of three separate experiments, each performed with six replicates for each condition. *$p < 0.05$, **$p < 0.01$, ***$p < 0.001$.

To gain an understanding of the structural characteristics, we used high resolution STEM imaging to examine 0N4R tau aggregates following 40hr incubation in the presence or absence of 20μM PLGA. Our results showed that native PLGA nanoparticles were associated directly with the tau fibers. In addition, while tau fibrils in the absence of PLGA presented as long, elongated fibers, PLGA-treated samples displayed a more heterogenous population of shorter twisted fibers, indicating a potential transition towards or the formation of shorter fibrils (Figure 3D, E, I, J, N, O, S and T). This conformational shift of 0N4R tau aggregates is evident more at 37°C and 40°C than at 27°C or 34°C. The reduction of elongated insoluble fibrils was supported by our BCA assay, which showed that soluble tau protein content was increased as a function of PLGA concentrations (5, 10, 20μM) compared to PLGA untreated samples after incubation at 27°C, 34°C, 37°C and 40°C (Figure 3W). To substantiate the decrease in the overall size of 0N4R tau aggregates following incubation with 20μM PLGA at different temperatures, we performed DLS analysis of tau samples after the ThT kinetic assay. A significant reduction in the hydrodynamic radii of tau aggregates was evident upon PLGA treatment, leading to the emergence of multiple peaks at different temperature conditions. The significant decrease in the hydrodynamic radii of tau aggregates was found to be more obvious at 37°C and 40°C than those observed at 27°C or 34°C, reinforcing our other biophysical results (Figure 4A–H).

Our kinetic data, DLS analysis and fluorescence imaging of ThT assay samples showed that native PLGA, as observed with 0N4R tau, dose-dependently (5, 10, 20μM) suppressed the spontaneous aggregation of 10μM 2N4R tau. At 5 and 10μM of PLGA, the effect was significant but a more pronounced suppressive response was apparent at 20μM PLGA (Supplementary Figure 1E–H). It is also of interest to note that 20μM native PLGA attenuated aggregation of 2N4R tau more noticeably than that of equimolar concentrations of 0N4R tau over the same 40hr incubation period at 37°C (Supplementary Figure 1I–K).

## Effects of PLGA on Temperature-Dependent Tau Disassembly

To investigate if native PLGA can trigger disassembly of matured tau fibers, we performed various assays using preformed 0N4R tau fibers with or without 20μM PLGA at different temperatures (ie, 27°C, 34°C, 37°C and 40°C) (Figures 5A–V and 6A–H). Our ThT kinetic results revealed that disaggregation of matured tau fibers was initially facilitated by PLGA at all temperatures as a function of time and then remained stable over the 60hr incubation period (Figure 5A, F, K and P). It is of interest to note that the dissociation rate increased significantly with temperature, leading to differences in the relative levels of disassembled tau fibers (ie, 18.4% at 27°C, 32.6% at 34°C, 33.8% at 37°C and 50.5% at 40°C) following 60hr incubation at various temperatures (Figure 5U and V). This was partly substantiated by our fluorescence imaging data which showed temperature-dependent reduction of matured 0N4R tau fibrils following PLGA treatment (Figure 5B, C, G, H, L, M, Q and R). Our STEM images also demonstrated a relative decrease in the quantity and size of 0N4R tau fibers at higher temperatures (Figure 5D, E, I, J, N, O, S and T). Additionally, DLS analysis of disassembled tau samples obtained following PLGA-treatment displayed a significant shift towards smaller aggregates (hydrodynamic radii ~200 to 1000nm) compared to untreated tau aggregates (hydrodynamic radii ~3000 to 4000nm). This size shift was more pronounced at 37°C and 40°C than at 27°C or 34°C, as observed with other experimental paradigms (see Figure 6A–H).

## Effects of PLGA on Different Tau Conformers

To assess possible interactions between PLGA and tau aggregation motifs, we performed an ANS assay, which is commonly used to detect hydrophobic clusters in protein and protein aggregates. An observed increase in ANS fluorescence is likely due to direct interaction of the aggregation prone PHF6 and PHF6* hexapeptide motifs of two tau molecules.[72] Conversely, we noted a significant decrease in fluorescence intensity in the presence of PLGA nanoparticles, suggesting a potential hydrophobic interaction between 0N4R tau and native PLGA (Figure 7A). Subsequently, to evaluate the effects of PLGA on various 0N4R tau conformers, we first confirmed the aggregate sizes of our monomeric, oligomeric and fibrillar tau preparations using the AF4. The crossflow gradient was set to separate particles ranging from 3 to 300nm R_H within a 60min run as described earlier.[68] For all samples, we injected 150μg of total protein. The elution profile was monitored by static light scattering at 90° (LS 90°), and the R_H of the eluting particles was measured by in-line DLS. Monomeric 0N4R tau (Figure 7B, red curve) eluted in the first 20min,
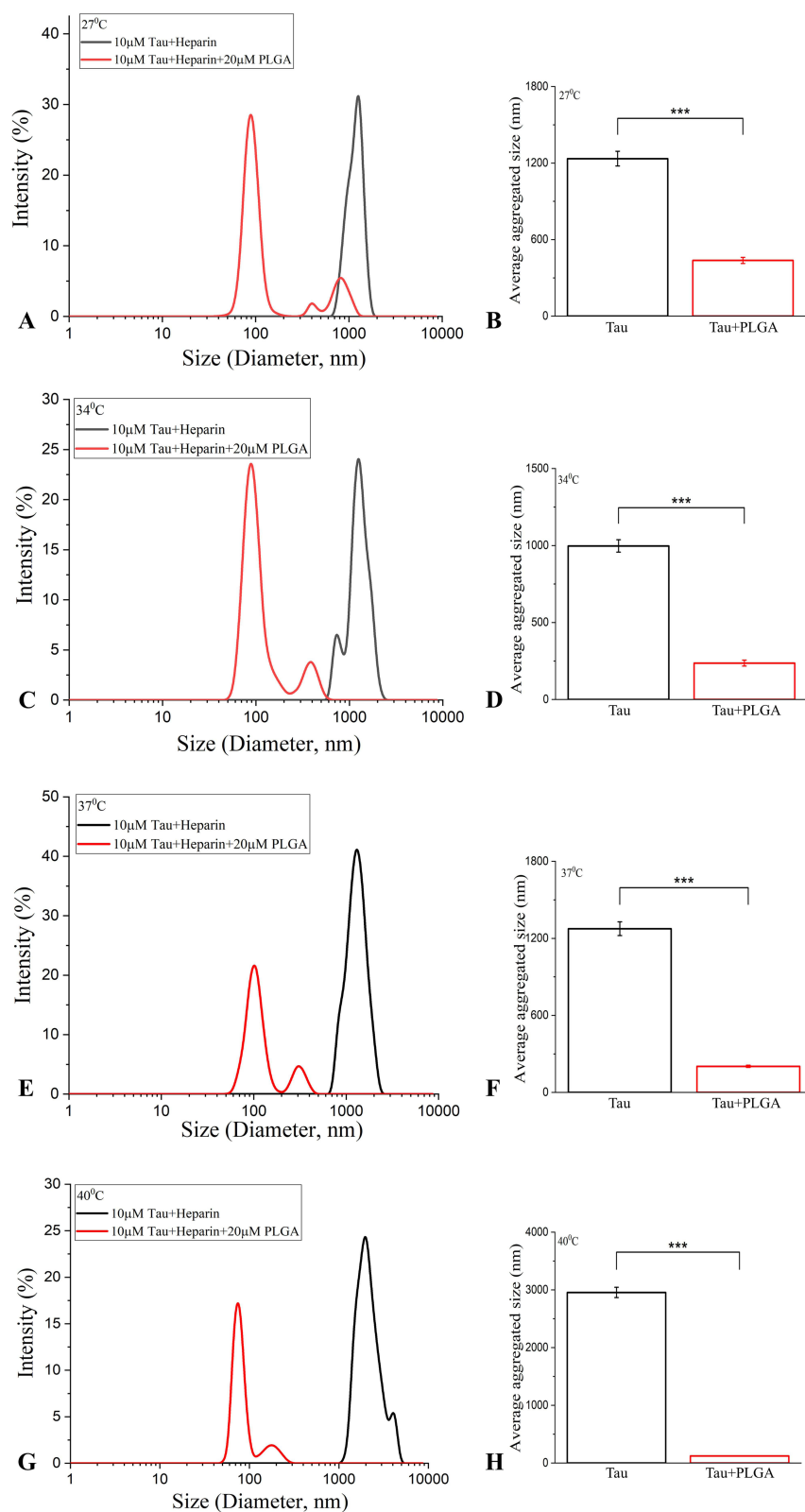
Figure 4 DLS analysis of tau aggregation in the presence of PLGA at different temperatures. (**A**–**H**) DLS analysis of 10μM 0N4R tau in the presence and absence of 20μM PLGA following 40hr incubation at 27°C (**A** and **B**), 34°C (**C** and **D**), 37°C (**E** and **F**) and 40°C (**G** and **H**). Note the significant decrease in the diameter of tau aggregates in the presence of 20μM PLGA as a function of increase in temperature from 27°C to 40°C, compared to control tau as depicted by size distribution curves and respective histograms representing average sizes of tau aggregates for a given concentration. ***$p < 0.001$.
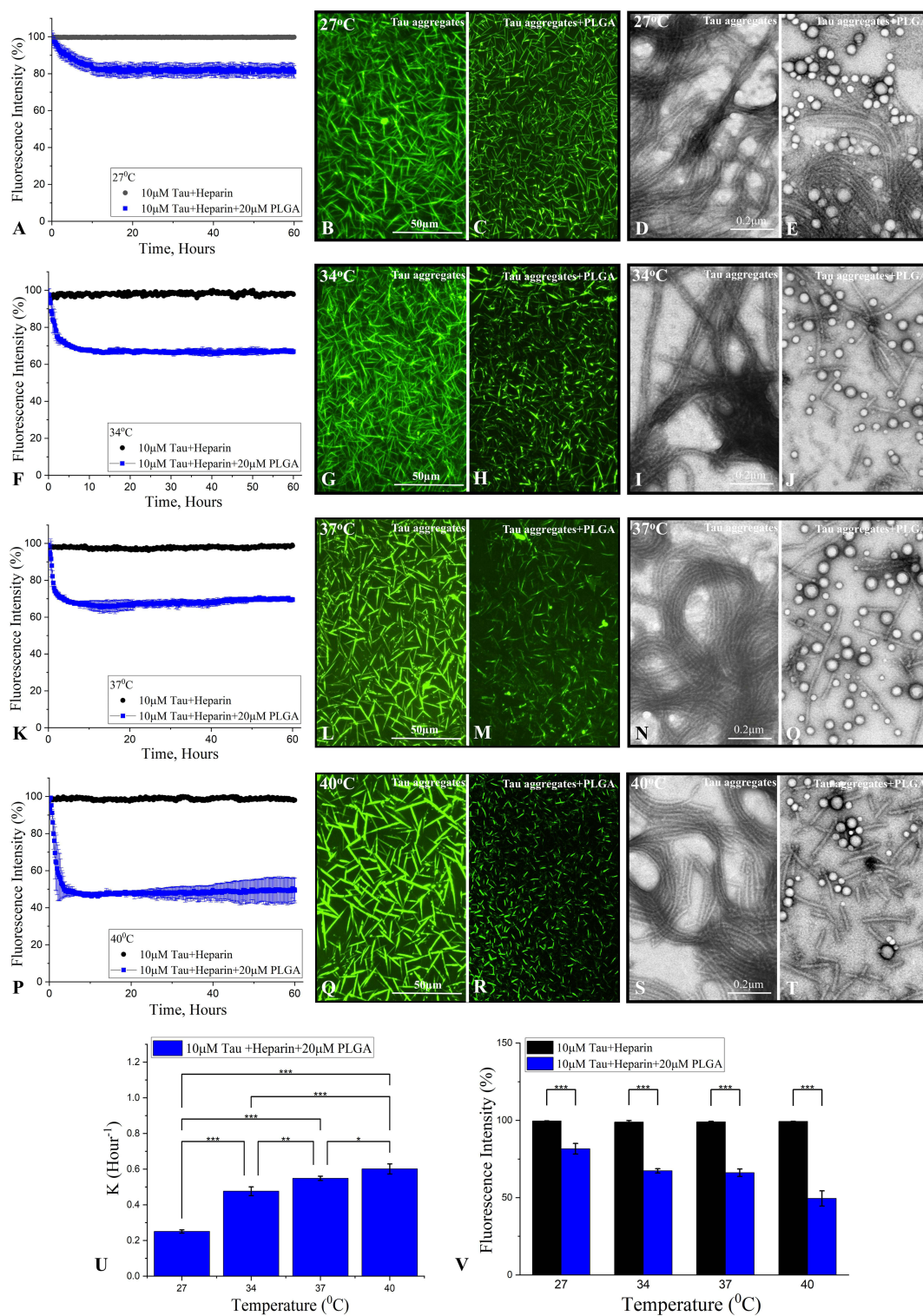
Figure 5 Attenuation of pre-aggregated tau fibers by PLGA at different temperatures. (**A–V**) ThT kinetic assays showing the disassembly of matured tau fibers and the corresponding fluorescence as well as STEM images in the absence and presence of 20μM PLGA over 60hr incubation at 27°C (**A–E**), 34°C (**F–J**), 37°C (**K–O**) and 40°C (**P–T**). A faster rate of tau disaggregation was evident in ThT kinetic experiment with the rise of temperature. Note the decrease in tau aggregates following 60hr incubation in the presence of PLGA as evident in the fluorescence as well as STEM images at various temperature. The presence of PLGA nanoparticles (round structures) was apparent in conjugation with disassembled tau fibers at different temperatures. (**U** and **V**) Histograms representing the kinetics of tau disassembly (**U**) and significant attenuation of fluorescence values at saturation (**V**) of tau kinetic reaction in the absence and presence of 20μM PLGA at different temperatures. All ThT kinetic graphs represented average mean ± SEM of three separate experiments, each performed with six replicates for each condition. *$p < 0.05$, **$p < 0.01$, ***$p < 0.001$.
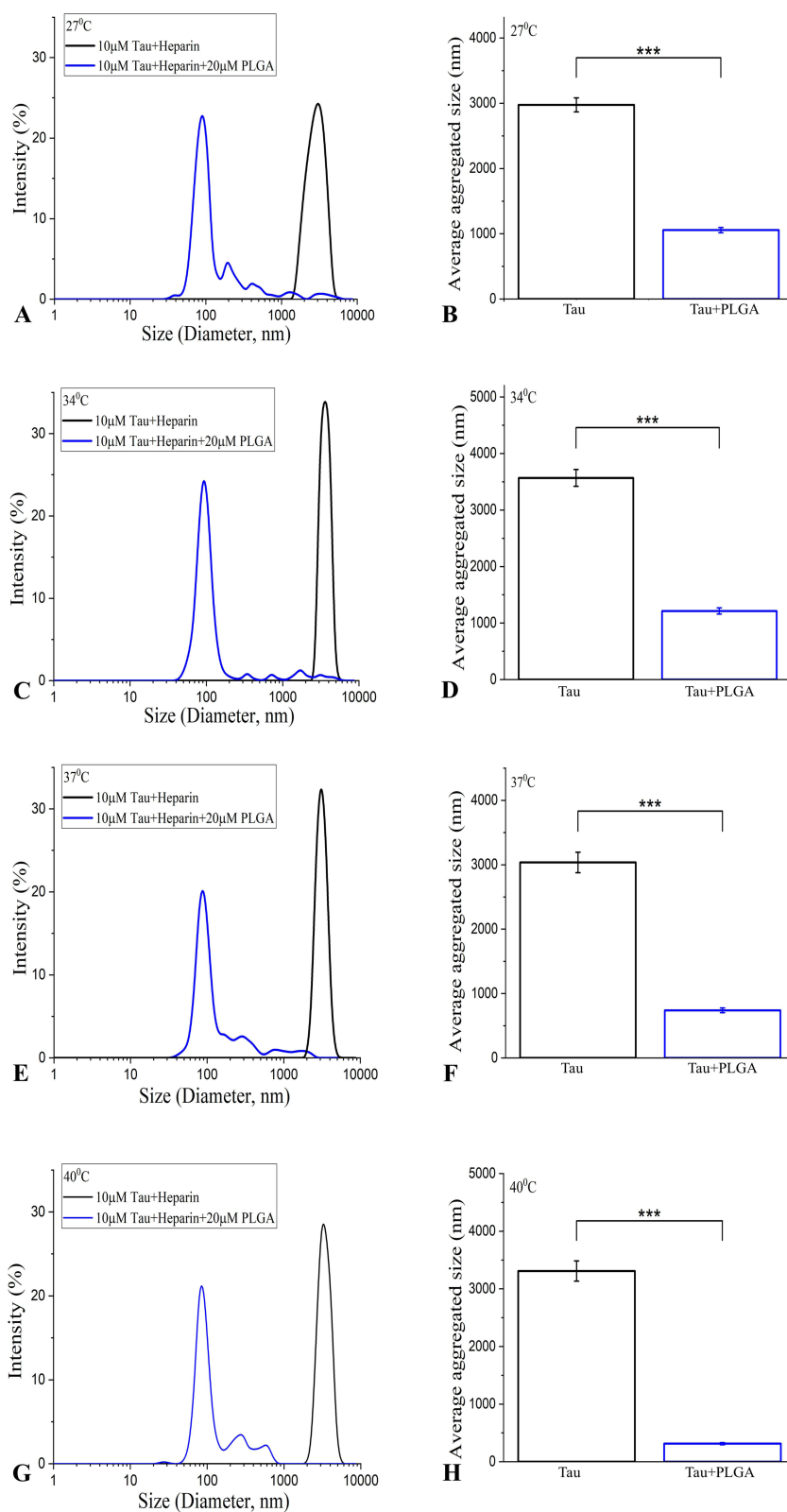
Figure 6 DLS analysis of tau disassembly by PLGA at different temperatures. (**A**–**H**) DLS analysis showing the disassembly of matured tau fibers in the presence and absence of 20μM PLGA following 60hr incubation at 27°C (**A** and **B**), 34°C (**C** and **D**), 37°C (**E** and **F**) and 40°C (**G** and **H**). Note the significant decrease in the tau aggregates diameter in the presence of 20μM PLGA with an increase in temperature from 27°C to 40°C compared to control tau aggregates as revealed by size distribution curves and respective histograms representing average sizes of tau aggregates for a given concentration. ***$p < 0.001$.
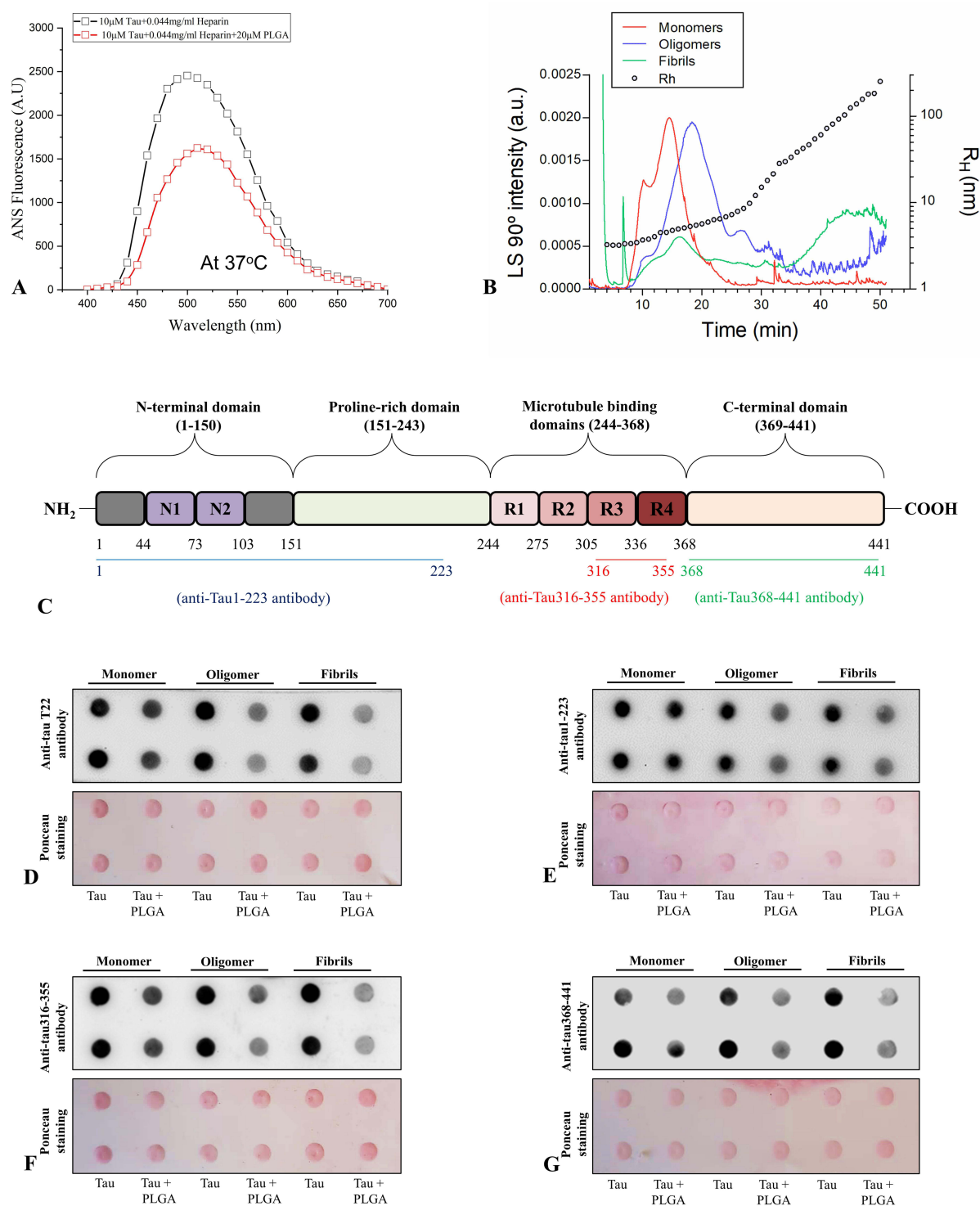
Figure 7 Characterization of PLGA interaction with 0N4R tau protein. (**A**) Fluorescence emission spectra of ANS after binding to aggregates of tau alone and in the presence of 20μM PLGA. Note the decrease in the intensity of fluorescence emission spectra in the presence of PLGA. (**B**) Fractograms of the monomeric (red), oligomeric (blue), and fibrillar (green) forms of tau. The solid curves represent the static light scattering intensity at 90° of the eluted samples, while the circles indicate the averaged hydrodynamic radius (Rh) from thirty DLS measurements taken during the one-minute collection period. (**C**) Diagram depicting the structure of the longest isoform of human tau (2N4R) present in the brain, which differs from other isoforms in the presence or absence of two N-terminal domains (0N, 1N Exon 2, 2N Exons 2 and 3), central Proline-rich domain (PRD) and one of the repeats in the microtubule interaction domain (3R or 4R by alternative splicing at Exon 10). (**D–G**) Dot blot assay showing the interaction of different conformers of tau (monomer, oligomer and fibril) in the absence and presence of 20μM PLGA as detected using region-specific (ie, Tau1-223; Tau316-355 and Tau368-441) as well as oligomeric T22 antibodies. The corresponding dot-blots were stained with Ponceau to depict loading of tau samples. Note that PLGA interacts somewhat more with oligomeric and fibrillar isoforms of tau than with the monomeric isoform, and this is mediated possibly via MTBD and CTD of the tau protein.

with a peak at 15min corresponding to a size of approximately 4.5nm R_H. Oligomeric 0N4R tau (Figure 7B, blue curve) eluted between 12 and 30min, with a main peak at 18min corresponding to an R_H of 5.5nm, and a minor peak at 26min corresponding to an R_H of 8nm. The LS 90° signal began to increase after 45min of elution for the fibrillar preparation (Figure 7B, green curve), indicating the presence of 0N4R tau aggregates ranging from 30 to 300nm R_H. The fibrillar preparation also exhibited a small peak in the oligomeric region. Having confirmed monomeric, oligomeric and fibrillar predominance in our respective 0N4R tau preparations, we incubated the samples with or without 20µM native PLGA and performed a filter-trap assay using various site-specific tau antibodies (Figure 7C). Our results demonstrated that PLGA attenuated antibody binding more predominantly for oligomeric and fibrillar 0N4R tau preparations than for monomers. Furthermore, the binding of tau antibody recognizing NTD and PRD (ie, anti-tau1-223) was less affected by PLGA than that observed with antibodies recognizing MTBD and CTD (ie, anti-tau316-355 and anti-tau368-441) (Figure 7D–G). This raises the possibility that native PLGA interacts primarily via the MTBD and CTD regions of the protein.

Discussion

The current study used biophysical, biochemical and structural studies to show that native PLGA nanoparticles without conjugation to any drug/agent can attenuate the temperature-dependent aggregation of tau protein. This is supported by results which show that: i) aggregation propensity of 0N4R tau increases significantly in a concentration-dependent manner with a rise in temperature from 27°C to 40°C, ii) native PLGA significantly attenuates tau aggregation in a dose-dependent manner at all studied temperatures, iii) inhibition of tau aggregation by PLGA is likely mediated by interaction with MTBD and CTD regions of the tau protein, iv) native PLGA can differentially trigger disassembly of pre-aggregated tau at various temperatures and v) PLGA nanoparticles, apart from 0N4R tau, also attenuate aggregation of 2N4R tau in a dose-dependent manner. Collectively, these results suggest that native PLGA can markedly inhibit tau aggregation and trigger disassembly of aggregated tau at physiological and non-physiological temperature ranges, suggesting its inimitable potential in the treatment of tau-related pathology.

Evidence suggests that increased phosphorylation and/or other posttranslational modifications initiate an alteration in the MTBD of tau, leading to conversion of the monomeric form to a pathological fibrillar aggregate displaying a characteristic cross-β structure with stacking of β strands perpendicular to the long fiber axis.[4,73] The first step in the conversion involves dimerization of tau protein occurring either by intermolecular disulfide crosslinking between cystine[291] and cystine[322] residues located in the R2 and R3 domains respectively or by electrostatic interactions between the negatively charged NTD and the positively charged PRD and MTBD. The tau dimers then self-assemble via the aggregation-prone hexapeptide motifs, [275]VQIINK[280] (PHF6*) and [306]VQIVYK[311] (PHF6) residing on the R2 and R3 repeats of the MTBD, to form oligomers which subsequently acquire fibrillar β-sheet structure generating PHFs - the building blocks of NFTs.[74–76] Interestingly, full-length recombinant tau, due to its hydrophilic nature and lack of post-translational modifications, shows very little intrinsic tendency to aggregate under normal conditions.[72,73] Nevertheless, aggregation of tau can be induced under in vitro in the presence of polyanionic factors such as heparin, RNA and arachidonic acid which by activating VQIVYK/VQIINK motifs promote conformational change from random coils to β-sheet structures, leading to the formation of tau filaments.[2,7,11,77] In fact, heparin-induced aggregation of recombinant tau has been studied in vitro not only to understand the mechanisms of tau fibrillization but also to examine factors/agents that can regulate tau aggregation. Our present results show that formation of heparin-induced tau fibrils is enhanced in vitro with increasing protein concentration as well as a rise in temperature from 27°C to 40°C as apparent by our ThT kinetic assay, fluorescence and electron microscopy studies. The duration of the lag phase is significantly reduced as a function of protein concentration as well as temperature, whereas the fibril exponential phase is decreased with the rise of temperature at a given concentration of tau. The subsequent saturation phase, on the other hand, escalated predominantly with the increased concentration of the protein – suggesting that earlier phases of kinetic reactions are more thermodynamically dependent than the saturation phase of tau fibrillation. Thus, it appears from our ThT binding assays that temperature most likely accelerates the rate of fibril formation but not the total tau fibrillar content. This is consistent with the reported effects of temperature on the aggregation of various other proteins, including Aβ peptide,

demonstrating the importance of ionic and hydrophobic interactions that underlie the formation of β-sheet structure associated with tau aggregation.[62,70,71,78]

Although aggregation of tau protein is known to be influenced by temperature variations, very little is known about whether the presence of any nanoparticles or small molecules can impact temperature-dependent tau fibrillation. This is important for the treatment of tau pathology as the local temperatures in the brain vary noticeably from 33.4°C to 42°C in disease/pathological conditions.[28,79,80] There is evidence that some nanoparticles functionalized with inhibitors such as methylene blue, nicotinamide or curcumin can attenuate tau pathology by improving blood-brain barrier permeability, binding affinity and/or regulating tau kinases.[56,81–83] However, no information is currently available if any nanoparticles without conjugation to any drug/agent can affect tau aggregation kinetics as a function of temperature variation. The present study reveals that native PLGA can attenuate temperature-dependent tau fibrillation as apparent by ThT kinetic assays, fluorescence imaging, STEM and DLS analyses showing the generation of shorter and fragmented tau fibrils with reduced hydrodynamic radius. The dose-dependent inhibitory effects of PLGA on the growth/saturation phases of tau fibrils was apparent at all temperatures studied, but the effect of PLGA on lag phase was most apparent at 40°C, suggesting that three stages of tau fibrillation may be differentially affected by native PLGA depending on the temperature. It is of interest to note that suppression of tau aggregation by native PLGA was directly proportional to the rise of temperature from 27°C to 40°C. This could be due to the interaction of PLGA with MTBD and CTD precluding the formation of critical nuclei and subsequent elongation of fibrils by preventing hydrogen bonding and hydrophobic interactions. This is partly supported by a decrease in the ANS fluorescence intensity in the presence of PLGA, suggesting existence of less solvent exposed hydrophobic clusters in tau aggregates. The interaction of PLGA with monomers and/or destabilizing the initial assembly of β-sheets during nucleation may also contribute to the attenuation of tau fibril formation. Additionally, PLGA can inhibit the tau oligomer formation by hydrophilic or electrostatic interactions, resulting in destabilization of on-pathway and formation of off-pathway soluble tau intermediates. This is partly supported by our filter-trap analysis showing an attenuation of tau oligomer and fibrillar contents suggesting the presence of non-fibrillar tau following exposure to native PLGA. It is of interest to note that native PLGA, apart from 0N4R tau, can suppress 2N4R tau aggregation in a dose-dependent manner, indicating that the effects of the nanoparticles may be independent of various tau isoforms present in the brain.

Apart from decreasing spontaneous aggregation, native PLGA was found to trigger significant disassembly of pre-aggregated tau fibers into smaller species at all temperatures over a 60hr period. The kinetic rate and the magnitude of tau fiber disassembly increased with a rise of temperature from 27°C to 40°C. Since MTBD of tau is positively charged,[3,76] the increased negative charge density on the surface of PLGA may promote a stronger electrostatic interaction with the tau protein, which could trigger disassembly of the preformed fibrillar structure. It is possible that native PLGA may trigger disassembly by interfering with the hydrophilic bonding with the MTBD region of the aggregated tau or the ensuing steric zipper interface within the cross β-spine. Additionally, the non-covalent bonding, ie, charge–charge interactions and hydrogen bonding between PLGA and tau fibrils may influence the disassembly of the preformed fibrillar structure.[77] It is however, important to emphasize that our in vitro studies showing the influences of temperatures on tau aggregation/disaggregation can not be co-related directly to in vivo results which are regulated by a complex interplay of numerous endogenous factors. This is evident from the fact that while acute higher body temperatures, such as those experienced in a sauna, are associated with lower tau pathology,[22] sustained higher body temperatures may lead to increased tau pathology.[26,39] Similar phenomena have been reported using a variety of phytochemicals, peptides and polymers including curcumin, clioquinol, epigallocatechin gallate, polyproline and myricetin.[57,84–88]

Accompanying aging, hypothermia has long been proposed as a risk factor for AD based on the observation that elderly people have a tendency to display cold intolerance and the evidence that Down syndrome patients who invariably develop AD exhibit a decrease in body temperature compared to age-matched normal individuals.[89,90] Interestingly, the 3xTgAD mouse model of AD is also reported to exhibit a lower body temperature at 12–14 months of age compared to control mice.[25] Over the years, multiple lines of experimental approaches including animal models of AD, hibernating animals and the use of anesthetics suggest that cold temperatures can increase tau phosphorylation and/or fibrillogenesis, whereas increasing temperature by deleting uncoupling protein 1, exposing to sauna-like conditions or menthol treatment have been shown to differentially affect tau pathology.[21,22,34,35,38,39,91] Altered tau phosphorylation has been ascribed to

altered tau kinases and/or phosphatases along with a failure in tau degradation via the proteasomal pathway.[20,21,92,93] At present, however, very little is known on whether temperature-dependent tau phosphorylation/aggregation can be influenced by an agent/drug that may have the potential to treat AD-related pathology. We have recently reported that native PLGA can attenuate Aβ aggregation at various temperatures.[62] Furthermore, PLGA was found to protect cultured mouse neurons as well as neurons derived from AD patients against Aβ toxicity by reducing tau kinases/phosphorylation.[60–62,94] Consistent with these results, the present study demonstrates that PLGA nanoparticles can inhibit not only spontaneous aggregation but also can trigger disassembly of aggregated tau at various temperatures (ie, 27°C to 40°C). The beneficial effects of native PLGA on tau aggregation/disassembly, as observed with the Aβ peptide, appear to improve with the rise of temperatures. Given the evidence that mild hyperthermia can affect tau pathology differentially in cellular/animal models,[22,39] we believe that native PLGA that target distinct facets of tau pathology will offer a new prospect to treat diseases associated with tauopathies including AD.

Conclusions

Our study reveals that spontaneous aggregation of tau protein increases in a concentration-dependent manner with a rise in temperature from 27°C to 40°C, as evaluated using a variety of biophysical, structural and biochemical assays. PLGA nanoparticles without conjugation to any drug/agent can significantly attenuate the propensity of tau to aggregate at all temperatures in a dose-dependent manner, most likely by interacting with the aggregation-prone hydrophobic hexapeptide motifs of the tau protein. Additionally, PLGA is able to trigger disaggregation of preformed tau aggregates as a function of temperature from 27°C to 40°C. Given the evidence that temperature plays an important role in regulating tau pathology, we believe that native PLGA may have therapeutic potential for tau-related pathologies.

Abbreviations

Aβ, amyloid β; AD, Alzheimer's disease; AF4, Asymmetric-flow field-flow fractionation; ANS, 8-anilino-1-naphthalene sulfonate; BCA, bicinchoninic acid; CTD, C-terminal domain; DLS, dynamic light scattering; DMSO, dimethyl sulfoxide; DTT, Dithiothreitol; ECL, enhanced chemiluminescence; MAPT, microtubule associated protein tau; MTBD, microtubule binding domain; NFT, intracellular neurofibrillary tangles; NTD, N-terminal domain; PRD, proline-rich domain; PBS, phosphate-buffered saline; PHFs, paired helical filaments; PLGA, poly(D,L-lactide-co-glycolide); STEM, scanning transmission electron microscopy; ThT, Thioflavin-T.

Data Sharing Statement

The data in this work are available in the manuscript or available from the corresponding author upon reasonable request.

Author Contributions

All authors made a significant contribution to the work reported, whether that is in the conception, study design, execution, acquisition of data, analysis and interpretation, or in all these areas; took part in drafting, revising or critically reviewing the article; gave final approval of the version to be published; have agreed on the journal to which the article has been submitted; and agree to be accountable for all aspects of the work.

Funding

Disclosure

The authors declare no conflicts of interest or personal relationships that could have appeared to influence the work reported in this paper.

References

1. Mandelkow EM, Mandelkow E. Biochemistry and cell biology of tau protein in neurofibrillary degeneration. *Cold Spring Harb Perspect Med*. 2012;2(7):a006247. doi:10.1101/cshperspect.a006247

2. Brandt R, Trushina NI, Bakota L. Much more than a cytoskeletal protein: physiological and pathological functions of the non-microtubule binding region of tau. *Front Neurol*. 2020;11:590059. doi:10.3389/fneur.2020.590059

3. Melková K, Zapletal V, Narasimhan S, et al. Structure and functions of microtubule associated proteins tau and MAP2c: similarities and differences. *Biomolecules*. 2019;9:105. doi:10.3390/biom9030105

4. Wang Y, Mandelkow E. Tau in physiology and pathology. *Nat Rev Neurosci*. 2016;17:5–21. doi:10.1038/nrn.2015.1

5. Ballatore C, Lee VM, Trojanowski JQ. Tau-mediated neurodegeneration in Alzheimer's disease and related disorders. *Nat Rev Neurosci*. 2007;8:663–672. doi:10.1038/nrn2194

6. Wang JZ, Xia YY, Grundke-Iqbal I, et al. Abnormal hyperphosphorylation of tau: sites, regulation, and molecular mechanism of neurofibrillary degeneration. *J Alzheimers Dis*. 2013;33(Suppl 1):S123–39. doi:10.3233/JAD-2012-129031

7. Goedert M, Spillantini MG. Ordered assembly of tau protein and neurodegeneration. *Adv Exp Med Biol*. 2019;1184:3–21. doi:10.1007/978-981-32-9358-8_1

8. Kent SA, Spires-Jones TL, Durrant CS. The physiological roles of tau and Aβ: implications for Alzheimer's disease pathology and therapeutics. *Acta Neuropathol*. 2020;140:417–447. doi:10.1007/s00401-020-02196-w

9. Mudher A, Colin M, Dujardin S, et al. What is the evidence that tau pathology spreads through prion-like propagation? *Acta Neuropathol Commun*. 2017;5:99. doi:10.1186/s40478-017-0488-7

10. Gibbons GS, Lee VMY, Trojanowski JQ. Mechanisms of cell-to-cell transmission of pathological tau: a review. *JAMA Neurol*. 2019;76 (1):101–108. doi:10.1001/jamaneurol.2018.2505

11. Zeng Y, Yang J, Zhang B, et al. The structure and phase of tau: from monomer to amyloid filament. *Cell Mol Life Sci*. 2021;78:1873–1886. doi:10.1007/s00018-020-03681-x

12. Seitkazina A, Kim KH, Fagan E, et al. The fate of tau aggregates between clearance and transmission. *Front Aging Neurosci*. 2022;14:932541. doi:10.3389/fnagi.2022.932541

13. Park S, Lee JH, Jeon JH, et al. Degradation or aggregation: the ramifications of post-translational modifications on tau. *BMB Rep*. 2018;51:265–273. doi:10.5483/bmbrep.2018.51.6.077

14. Alquezar C, Arya S, Kao AW. Tau post-translational modifications: dynamic transformers of tau function, degradation and aggregation. *Front Neurol*. 2020;11:595532. doi:10.3389/fneur.2020.595532

15. Ye H, Han Y, Li P, et al. The Role of post-translational modifications on the structure and function of tau protein. *J Mol Neurosci*. 2022;72:1557–1571. doi:10.1007/s12031-022-02002-0

16. Jebarupa B, Muralidharan M, Srinivasu BY, et al. Effect of altered solution conditions on tau conformational dynamics: plausible implication on order propensity and aggregation. *Biochim Biophys Acta Proteins Proteom*. 2018;1866:668–679. doi:10.1016/j.bbapap.2018.04.004

17. Kim AC, Lim S, Kim YK. Metal ion effects on Aβ and tau aggregation. *Int J Mol Sci*. 2018;19:128. doi:10.3390/ijms19010128

18. Ahmadi S, Zhu S, Sharma R, et al. Aggregation of microtubule binding repeats of tau protein is promoted by Cu^2. *ACS Omega*. 2019;4:5356–5366. doi:10.1021/acsomega.8b03595

19. Roman AY, Devred F, Byrne D, et al. Zinc induces temperature-dependent reversible self-assembly of tau. *J Mol Biol*. 2019;431:687–695. doi:10.1016/j.jmb.2018.12.008

20. Planel E, Miyasaka T, Launey T, et al. Alterations in glucose metabolism induce hypothermia leading to tau hyperphosphorylation through differential inhibition of kinase and phosphatase activities: implications for Alzheimer's disease. *J Neurosci*. 2004;24:2401–2411. doi:10.1523/JNEUROSCI.5561-03.2004

21. Bretteville A, Marcouiller F, Julien C, et al. Hypothermia-induced hyperphosphorylation: a new model to study tau kinase inhibitors. *Sci Rep*. 2012;2:480. doi:10.1038/srep00480

22. Guisle I, Canet G, Pétry S, et al. Sauna-like conditions or menthol treatment reduce tau phosphorylation through mild hyperthermia. *Neurobiol Aging*. 2022;113:118–130. doi:10.1016/j.neurobiolaging.2022.02.011

23. Su B, Wang X, Drew KL, et al. Physiological regulation of tau phosphorylation during hibernation. *J Neurochem*. 2008;105:2098–2108. doi:10.1111/j.1471-4159.2008.05294.x

24. Planel E, Bretteville A, Liu L, et al. Acceleration and persistence of neurofibrillary pathology in a mouse model of tauopathy following anesthesia. *FASEB J*. 2009;23:2595–2604. doi:10.1096/fj.08-122424

25. Vandal M, White PJ, Tournissac M, et al. Impaired thermoregulation and beneficial effects of thermoneutrality in the 3xTg-AD model of Alzheimer's disease. *Neurobiol Aging*. 2016;43:47–57. doi:10.1016/j.neurobiolaging.2016.03.024

26. Jung CG, Kato R, Zhou C, et al. Sustained high body temperature exacerbates cognitive function and Alzheimer's disease-related pathologies. *Sci Rep*. 2022;12:12273. doi:10.1038/s41598-022-16626-0

27. Corbett R, Laptook A, Weatherall P. Noninvasive measurements of human brain temperature using volume-localized proton magnetic resonance spectroscopy. *J Cereb Blood Flow Metab*. 1997;17:363–369. doi:10.1097/00004647-199704000-00001

28. Sukstanskii AL, Yablonskiy DA. Theoretical model of temperature regulation in the brain during changes in functional activity. *Proc Natl Acad Sci USA*. 2006;103:12144–12149. doi:10.1073/pnas.0604376103

29. Sinigaglia-Coimbra R, Cavalheiro EA, Coimbra CG. Postischemic hyperthermia induces Alzheimer-like pathology in the rat brain. *Acta Neuropathol*. 2002;103:444–452. doi:10.1007/s00401-001-0487-3

30. Ishigaki D, Ogasawara K, Yoshioka Y, et al. Brain temperature measured using proton MR spectroscopy detects cerebral hemodynamic impairment in patients with unilateral chronic major cerebral artery steno-occlusive disease: comparison with positron emission tomography. *Stroke*. 2009;40:3012–3016. doi:10.1161/STROKEAHA.109.555508

31. Ghavami M, Rezaei M, Ejtehadi R, et al. Physiological temperature has a crucial role in amyloid beta in the absence and presence of hydrophobic and hydrophilic nanoparticles. *ACS Chem Neurosci*. 2013;4:375–378. doi:10.1021/cn300205g

32. Laukkanen T, Kunutsor S, Kauhanen J, et al. Sauna bathing is inversely associated with dementia and Alzheimer's disease in middle-aged Finnish men. *Age Ageing*. 2017;46:245–249. doi:10.1093/ageing/afw212

33. Blessing EM, Parekh A, Betensky RA, et al. Association between lower body temperature and increased tau pathology in cognitively normal older adults. *Neurobiol Dis*. 2022;171:105748. doi:10.1016/j.nbd.2022.105748

34. Planel E, Richter KE, Nolan CE, et al. Anesthesia leads to tau hyperphosphorylation through inhibition of phosphatase activity by hypothermia. *J Neurosci*. 2007;27:3090–3097. doi:10.1523/JNEUROSCI.4854-06.2007

35. Stieler JT, Bullmann T, Kohl F, et al. The physiological link between metabolic rate depression and tau phosphorylation in mammalian hibernation. *PLoS One*. 2011;6:e14530. doi:10.1371/journal.pone.0014530

36. Tang JX, Baranov D, Hammond M, et al. Human Alzheimer and inflammation biomarkers after anesthesia and surgery. *Anesthesiol*. 2011;115:727–732. doi:10.1097/ALN.0b013e31822e9306

37. Carrettiero DC, Santiago FE, Motzko-Soares AC, et al. Temperature and toxic tau in Alzheimer's disease: new insights. *Temperature*. 2015;2:491–498. doi:10.1080/23328940.2015.1096438

38. De Paula CA, Santiago FE, de Oliveira AS, et al. The Co-chaperone BAG2 mediates cold-induced accumulation of phosphorylated tau in SH-SY5Y cells. *Cell Mol Neurobiol*. 2015;36:593–602. doi:10.1007/s10571-015-0239-x

39. Jung CG, Yamashita H, Kato R, et al. Deletion of UCP1 in Tg2576 mice increases body temperature and exacerbates Alzheimer's disease-related pathologies. *Int J Mol Sci*. 2023;24:2741. doi:10.3390/ijms24032741

40. Doane TL, Burda C. The unique role of nanoparticles in nanomedicine: imaging, drug delivery and therapy. *Chem Soc Rev*. 2012;41:2885–2911. doi:10.1039/c2cs15260f

41. Kim D, Shin K, Kwon SG, et al. Synthesis and biomedical applications of multifunctional nanoparticles. *Adv Mater*. 2018;30:e1802309. doi:10.1002/adma.201802309

42. Zahin N, Anwar R, Tewari D, et al. Nanoparticles and its biomedical applications in health and diseases: special focus on drug delivery. *Environ Sci Pollut Res Int*. 2020;27:19151–19168. doi:10.1007/s11356-019-05211-0

43. Abdel-Mageed HM, AbuelEzz NZ, Radwan RA, et al. Nanoparticles in nanomedicine: a comprehensive updated review on current status, challenges and emerging opportunities. *J Microencapsul*. 2021;38:414–436. doi:10.1080/02652048.2021.1942275

44. Karunakaran G, Sudha KG, Ali S, et al. Biosynthesis of nanoparticles from various biological sources and its biomedical applications. *Molecules*. 2023;28:4527. doi:10.3390/molecules28114527

45. Danhier F, Ansorena E, Silva JM, et al. PLGA-based nanoparticles: an overview of biomedical applications. *J Control Release*. 2012;161:505–522. doi:10.1016/j.jconrel.2012.01.043

46. Mohammadi-Samani S, Taghipour B. PLGA micro and nanoparticles in delivery of peptides and proteins; problems and approaches. *Pharm Dev Technol*. 2015;20:385–393. doi:10.3109/10837450.2014.882940

47. Mir M, Ahmed N, Rehman AU. Recent applications of PLGA based nanostructures in drug delivery. *Colloids Surf B Biointerfaces*. 2017;159:217–231. doi:10.1016/j.colsurfb.2017.07.038

48. Zhong H, Chan G, Hu Y, et al. A comprehensive map of FDA-approved pharmaceutical products. *Pharmaceutics*. 2018;10:263. doi:10.3390/pharmaceutics10040263

49. Essa D, Kondiah PPD, Choonara YE, et al. The design of poly(lactide-co-glycolide) nanocarriers for medical applications. *Front Bioeng Biotechnol*. 2020;8:48. doi:10.3389/fbioe.2020.00048

50. Fornaguera C, Dols-Perez A, Calderó G, et al. PLGA nanoparticles prepared by nano-emulsion templating using low-energy methods as efficient nanocarriers for drug delivery across the blood-brain barrier. *J Control Release*. 2015;211:134–143. doi:10.1016/j.jconrel.2015.06.002

51. Cai Q, Wang L, Deng G, et al. Systemic delivery to central nervous system by engineered PLGA nanoparticles. *Am J Transl Res*. 2016;8:749–764. eCollection 2016.

52. Zhi K, Raji B, Nookala AR, et al. PLGA nanoparticle-based formulations to cross the blood-brain barrier for drug delivery: from R&D to cGMP. *Pharmaceutics*. 2021;13:500. doi:10.3390/pharmaceutics13040500

53. Na Y, Zhang N, Zhong X, et al. Polylactic-co-glycolic acid-based nanoparticles modified with peptides and other linkers cross the blood-brain barrier for targeted drug delivery. *Nanomedicine*. 2023;18:125–143. doi:10.2217/nnm-2022-0287

54. Jinwal UK, Groshev A, Zhang J, et al. Preparation and characterization of methylene blue nanoparticles for Alzheimer's disease and other tauopathies. *Curr Drug Deliv*. 2014;11:541–550. doi:10.2174/1567201810666131113102037

55. Wobst HJ, Sharma A, Diamond MI, et al. The green tea polyphenol (-)-epigallocatechin gallate prevents the aggregation of tau protein into toxic oligomers at substoichiometric ratios. *FEBS Lett*. 2015;589:77–83. doi:10.1016/j.febslet.2014.11.026

56. Vakilinezhad MA, Amini A, Akbari Javar H, et al. Nicotinamide loaded functionalized solid lipid nanoparticles improves cognition in Alzheimer's disease animal model by reducing tau hyperphosphorylation. *DARU*. 2018;26:165–177. doi:10.1007/s40199-018-0221-5

57. Kumar S, Krishnakumar VG, Morya V, et al. Nanobiocatalyst facilitated aglycosidic quercetin as a potent inhibitor of tau protein aggregation. *Int J Biol Macromol*. 2019;138:168–180. doi:10.1016/j.ijbiomac.2019.07.081

58. Zheng Q, Kebede MT, Kemeh MM, et al. Inhibition of the self-assembly of Aβ and of tau by polyphenols: mechanistic studies. *Molecules*. 2019;24:2316. doi:10.3390/molecules24122316

59. Gao C, Chu X, Gong W, et al. Neuron tau-targeting biomimetic nanoparticles for curcumin delivery to delay progression of Alzheimer's disease. *J Nanobiotechnol*. 2020;18:71. doi:10.1186/s12951-020-00626-1

60. Wang Y, Wu Q, Anand BG, et al. Significance of cytosolic cathepsin D in Alzheimer's disease pathology: protective cellular effects of PLGA nanoparticles against β-amyloid-toxicity. *Neuropathol Appl Neurobiol*. 2020;46:686–706. doi:10.1111/nan.12647

61. Anand B, Wu Q, Nakhaei-Nejad M, et al. Significance of native PLGA nanoparticles in the treatment of Alzheimer's disease pathology. *Bioact Mater*. 2022;17:506–525. doi:10.1016/j.bioactmat.2022.05.030

62. Paul PS, Choi JY, Wu Q, et al. Unconjugated PLGA nanoparticles attenuate temperature-dependent beta-amyloid aggregation and protect neurons against toxicity: implications for Alzheimer's disease pathology. *J Nanobiotechnology*. 2022;20:67. doi:10.1186/s12951-022-01269-0

63. Paul PS, Patel T, Cho JY, et al. Native PLGA nanoparticles attenuate Aβ-seed induced tau aggregation under *in vitro* conditions: potential implication in Alzheimer's disease pathology. *Sci Rep*. 2024;14:144. doi:10.1038/s41598-023-50465-x

64. Mok SA, Condello C, Freilich R, et al. Mapping interactions with the chaperone network reveals factors that protect against tau aggregation. *Nat Struct Mol Biol*. 2018;25:384–393. doi:10.1038/s41594-018-0057-1

65. Foroutanpay BV, Kumar J, Kang SG, et al. The effects of N-terminal mutations on beta-amyloid peptide aggregation and toxicity. *Neuroscience*. 2018;379:177–188. doi:10.1016/j.neuroscience.2018.03.014

66. Mallesh R, Khan J, Gharai PK, et al. Hydrophobic C-terminal peptide analog Aβ$_{31-41}$ protects the neurons from Aβ-Induced toxicity. *ACS Chem Neurosci*. 2024;15:2372–2385. doi:10.1021/acschemneuro.4c00032

67. Anand B, Wu Q, Karthivashan G, et al. Mimosine functionalized gold nanoparticles (Mimo-AuNPs) suppress β-amyloid aggregation and neuronal toxicity. *Bioact Mater*. 2021;6:4491–4505. doi:10.1016/j.bioactmat.2021.04.029

68. Cortez LM, Nemani SK, Duque Velásquez C, et al. Asymmetric-flow field-flow fractionation of prions reveals a strain-specific continuum of quaternary structures with protease resistance developing at a hydrodynamic radius of 15nm. *PLoS Pathog*. 2021;17:e1009703. doi:10.1371/journal.ppat.1009703

69. Biancalana M, Koide S. Molecular mechanism of Thioflavin-T binding to amyloid fibrils. *Biochim Biophys Acta*. 2010;1804:1405–1412. doi:10.1016/j.bbapap.2010.04.001

70. Ciasca G, Campi G, Battisti A, et al. Continuous thermal collapse of the intrinsically disordered protein tau is driven by its entropic flexible domain. *Langmuir*. 2012;28:13405–13410. doi:10.1021/la302628y

71. Devi S, Chaturvedi M, Fatima S, et al. Environmental factors modulating protein conformations and their role in protein aggregation diseases. *Toxicology*. 2022;465:153049. doi:10.1016/j.tox.2021.153049

72. Jeganathan S, von Bergen M, Mandelkow EM, et al. The natively unfolded character of tau and its aggregation to Alzheimer-like paired helical filaments. *Biochemistry*. 2008;47:10526–10539. doi:10.1021/bi800783d

73. Oakley SS, Maina MB, Marshall KE, et al. Tau filament self-assembly and structure: tau as a therapeutic target. *Front Neurol*. 2020;11:590754. doi:10.3389/fneur.2020.590754

74. von Bergen M, Barghorn S, Biernat J, et al. Tau aggregation is driven by a transition from random coil to beta sheet structure. *Biochim Biophys Acta*. 2005;1739:158–166. doi:10.1016/j.bbadis.2004.09.010

75. Penke B, Szűcs M, Bogár F. Oligomerization and conformational change turn monomeric β-amyloid and tau proteins toxic: their role in Alzheimer's pathogenesis. *Molecules*. 2020;25:1659. doi:10.3390/molecules25071659

76. Wang D, Huang X, Yan L, et al. The structure biology of tau and clue for aggregation and inhibitor design. *Protein J*. 2021;40:656–668. doi:10.1007/s10930-021-10017-6

77. Khan S, Hassan MI, Shahid M, et al. Nature's toolbox against tau aggregation: an updated review of current research. *Ageing Res Rev*. 2023;87:101924. doi:10.1016/j.arr.2023.101924

78. Cheon M, Chang I, Hall CK. Influence of temperature on formation of perfect tau fragment fibrils using PRIME20/DMD simulations. *Protein Sci*. 2012;21:1514–1527. doi:10.1002/pro.2141

79. Krol S, Macrez R, Docagne F, et al. Therapeutic benefits from nanoparticles: the potential significance of nanoscience in diseases with compromise to the blood-brain barrier. *Chem Rev*. 2013;113:1877–1903. doi:10.1021/cr200472g

80. Ghalandari B, Asadollahi K, Shakerizadeh A, et al. Microtubule network as a potential candidate for targeting by gold nanoparticle-assisted photothermal therapy. *Photochem Photobiol B*. 2019;192:131–140. doi:10.1016/j.jphotobiol.2019.01.012

81. Chen Q, Du Y, Zhang K, et al. Tau-targeted multifunctional nanocomposite for combinational therapy of Alzheimer's disease. *ACS Nano*. 2018;12:1321–1338. doi:10.1021/acsnano.7b07625

82. Singh NA, Bhardwaj V, Ravi C, et al. EGCG nanoparticles attenuate aluminum chloride induced neurobehavioral deficits, β-amyloid and tau pathology in a rat model of Alzheimer's disease. *Front Aging Neurosci*. 2018;10:244. doi:10.3389/fnagi.2018.00244

83. Rifaai RA, Mokhemer SA, Saber EA, et al. Neuroprotective effect of quercetin nanoparticles: a possible prophylactic and therapeutic role in Alzheimer's disease. *J Chem Neuroanat*. 2020;107:101795. doi:10.1016/j.jchemneu.2020.101795

84. Rane JS, Bhaumik P, Panda D. Curcumin inhibits tau aggregation and disintegrates preformed tau filaments. *J Alzheimers Dis*. 2017;60:999–1014. doi:10.3233/JAD-170351

85. Zhu L, Xu L, Wu X, et al. Tau-targeted multifunctional nanoinhibitor for Alzheimer's disease. *ACS Appl Mater Interfaces*. 2021;13:23328–23338. doi:10.1021/acsami.1c00257

86. Sonawane SK, Ahmad A, Chinnathambi S. Protein-capped metal nanoparticles inhibit tau aggregation in Alzheimer's disease. *ACS Omega*. 2019;4:12833–12840. doi:10.1021/acsomega.9b01411

87. Sonawane SK, Chidambaram H, Boral D, et al. EGCG impedes human Tau aggregation and interacts with Tau. *Sci Rep*. 2020;10:12579. doi:10.1038/s41598-020-69429-6

88. Gharb M, Nouralishahi A, Riazi A, et al. Inhibition of tau protein aggregation by a chaperone-like beta-boswellic acid conjugated to gold nanoparticles. *ACS Omega*. 2022;7:30347–30358. doi:10.1021/acsomega.2c03616

89. Holtzman A, Simon EW. Body temperature as a risk factor for Alzheimer's disease. *Med Hypotheses*. 2000;55:440–444. doi:10.1054/mehy.2000.1085

90. Almeida MC, Carrettiero DC. Hypothermia as a risk factor for Alzheimer disease. *Handb Clin Neurol*. 2018;157:727–735. doi:10.1016/B978-0-444-64074-1.00044-6

91. Feng Q, Cheng B, Yang R, et al. Dynamic changes of phosphorylated tau in mouse hippocampus after cold water stress. *Neurosci Lett*. 2005;388:13–16. doi:10.1016/j.neulet.2005.06.022

92. Maurin H, Lechat B, Borghgraef P, et al. Terminal hypothermic Tau.P301L mice have increased Tau phosphorylation independently of glycogen synthase kinase 3α/β. *Eur J Neurosci*. 2014;40:2442–2453. doi:10.1111/ejn.12595

93. Julien C, Marcouiller F, Bretteville A, et al. Dimethyl sulfoxide induces both direct and indirect tau hyperphosphorylation. *PLoS One*. 2012;7:e40020. doi:10.1371/journal.pone.0040020

94. Wu Q, Karthivashan G, Nakhaei-Nejad M, et al. Native PLGA nanoparticles regulate APP metabolism and protect neurons against β-amyloid toxicity: potential significance in Alzheimer's disease pathology. *Int J Biol Macromol*. 2022;219:1180–1196. doi:10.1016/j.ijbiomac.2022.08.148